Wavefront Sensing Simulation Using a Lateral Shearing Interferometer for Zernike Aberrations

Yuanzhang Yang

School of Electronics and Information Technology, Sun Yat-sen University

July 2025

Abstract

This study presents a computational simulation of wavefront sensing using a lateral shearing interferometer, following the principles outlined by Murty (1964), to analyze the interference patterns generated by various Zernike aberrations. The simulation models optical wavefronts through a 20 mm circular aperture, subjected to aberrations including defocus, coma, spherical aberration, and astigmatism, under both flat and wedged plate configurations. Interference patterns are computed using a 632.8 nm He-Ne laser, and a dynamic visualization illustrates defocus evolution. The results demonstrate characteristic fringe patterns for each aberration, validating the simulation's ability to characterize wavefront distortions. This work provides insights into optical metrology and supports applications in adaptive optics and lens design.

1 Introduction

Wavefront sensing is a critical technique in optical metrology, enabling the characterization of wavefront distortions in optical systems [1]. The lateral shearing interferometer, first described by Murty (1964), is a robust method for measuring wavefront aberrations by comparing a wavefront with a laterally shifted version of itself [2]. This technique is widely used in adaptive optics, telescope optics, and lens quality

assessment due to its simplicity and sensitivity to wavefront gradients. Zernike aberrations, represented by orthogonal polynomials, are standard for describing optical imperfections such as defocus, coma, and astigmatism [3].

The problem addressed in this study is to simulate the interference patterns produced by a lateral shearing interferometer for various Zernike aberrations, both with and without a wedged plate, and to visualize the dynamic evolution of defocus. The objective is to quantify how aberration amplitudes influence interference patterns and to validate the simulation against expected optical behavior. This simulation aids in understanding wavefront distortions and supports the development of optical systems requiring precise aberration correction.

2 Methods

2.1 Simulation Framework

The simulation was implemented in MATLAB, modeling a lateral shearing interferometer with a 20 mm circular aperture and a 632.8 nm He-Ne laser. The wavefront is sampled on a 500×500 grid, with Cartesian coordinates (x, y) converted to normalized radial (ρ) and azimuthal (θ) coordinates. A binary mask defines the aperture where $\rho \leq 1$. Unlike the physical model in the paper, after multiple simulations and comparisons, this simulation uses 1μm as the fixed optical path difference and a linear $10^{-3}x$ (m) optical path difference to equivalent the additional optical path difference generated by the wedge angle, in order to achieve the best experimental results.

2.2 Zernike Aberrations

Seven aberration cases were simulated: ideal plane, defocus, horizontal coma, vertical coma, primary spherical aberration, 0° astigmatism, and 45° astigmatism. The optical path difference (OPD, W) for each aberration is computed using Zernike polynomials [3]:

Defocus: $W = \sqrt{3}\left(2\rho^2 - 1\right)$

Horizontal coma: $W = \sqrt{8}\left(3\rho^2 - 2\rho\right)\cos\theta$

Vertical coma: $W = \sqrt{8}\left(3\rho^2 - 2\rho\right)\sin\theta$

Spherical: $W = \sqrt{5}\left(6\rho^4 - 6\rho^2 + 1\right)$

Astigmatism 0°: $W = \sqrt{6}\rho^2\cos\left(2\theta\right)$

Astigmatism 45°: $W = \sqrt{6}\rho^2\sin\left(2\theta\right)$

The OPD is scaled by the wavelength λ = 632.8 nm to define aberration amplitudes.

2.3 Interference Pattern Calculation

The interference pattern is calculated as:

$$I = 2\cdot\left(1+\cos\left(\Delta\phi\right)\right)\cdot \text{mask}, \Delta\phi = \frac{2\pi}{\lambda}\mathcal{D} \tag{1.1}$$

where $\mathcal{D}$ is the OPD shifted by the shear distance, and the mask ensures intensity is computed only within the aperture. For wedged plates, the linear tilt causes a linear term $10^{-3}x$ (m) added to the OPD.

2.4 Dynamic Visualization

A dynamic simulation was conducted for six classical Zernike aberrations: defocus, horizontal coma, vertical coma, spherical aberration, 0° astigmatism, and 45° astigmatism. For each aberration type, the Zernike amplitude was linearly varied from −2.0λ to +2.0λ over 40 frames, representing a gradual evolution of the wavefront

distortion. At each step, the corresponding interference pattern was calculated using a fixed optical path difference of 1.0 μm, and visualized within a circular aperture of 20 mm diameter. The resulting frames were compiled into individual animated GIFs, with a 0.15-second delay per frame, clearly illustrating the progression and symmetry of each aberration's effect on the interferogram, here are the key frames of different types of aberrations, COEF represents to the Zernike coefficients, which represents the coefficient multiplied by the Zernike polynomials under the corresponding types of aberrations.

• **Defocus**:

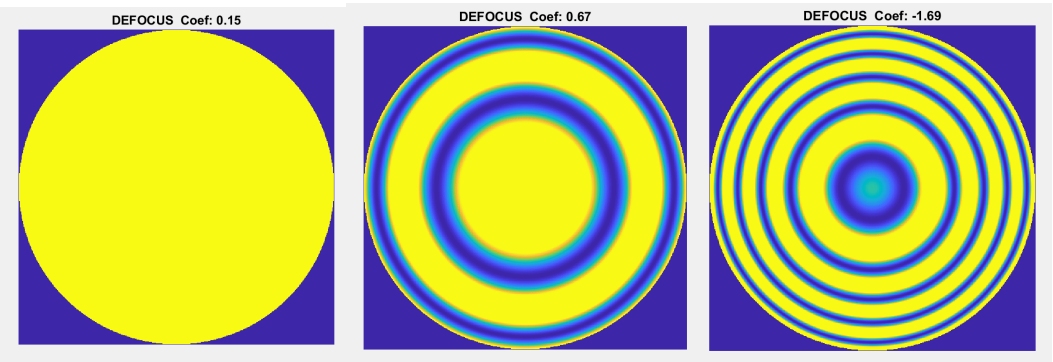

• **Horizontal coma**:

• **Vertical coma**:

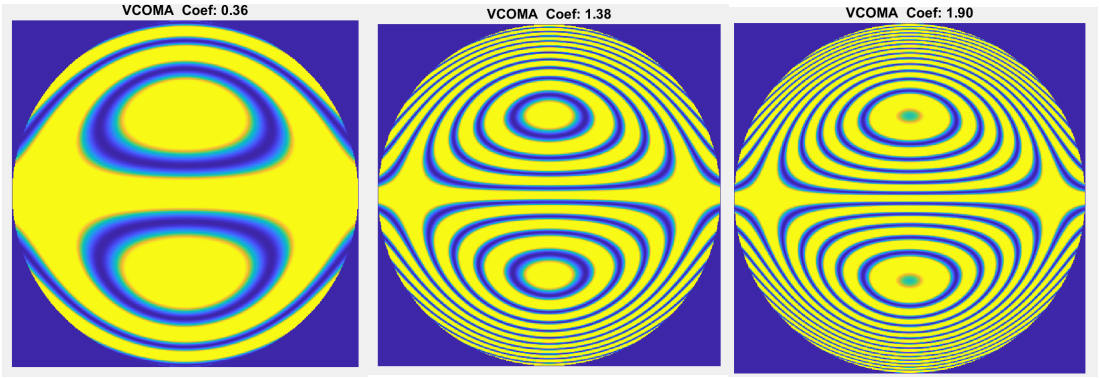

• **Spherical**:

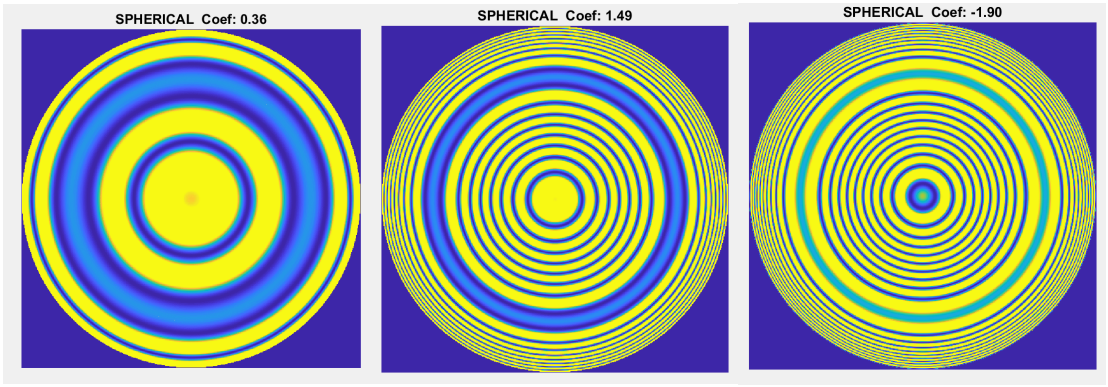

• **Astigmatism** 0° :

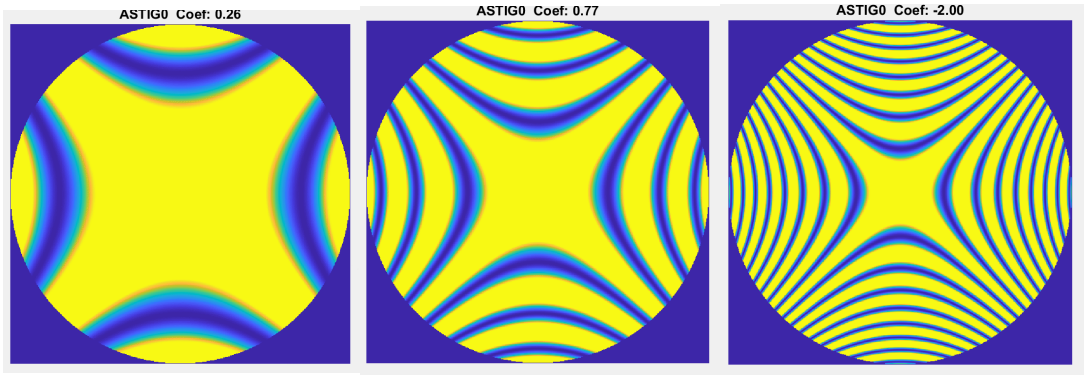

• **Astigmatism** 45° :

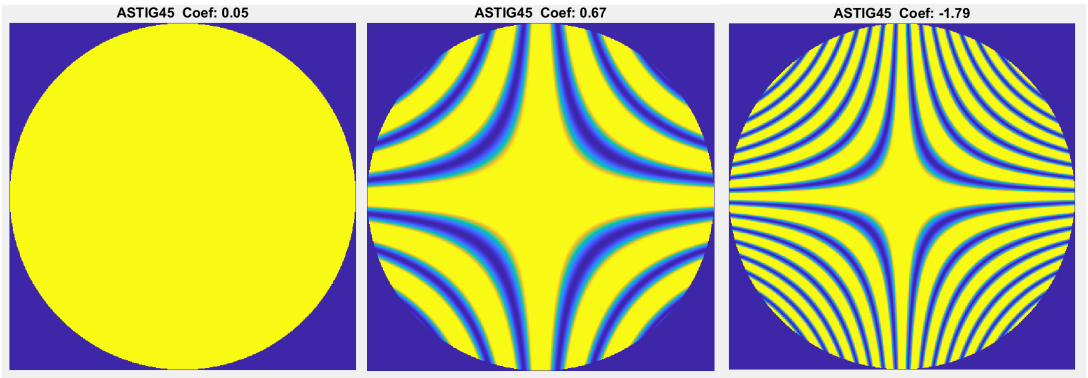

2.5 Visualization

Interference patterns were visualized using filled intensity plots over a circular aperture, with the Parula colormap applied uniformly across all frames. Each frame was rendered with publication-quality formatting, including Times New Roman font, 12 pt axis labels, and a 14 pt bold title. The spatial coordinates were expressed in millimeters, and the intensity was scaled and clipped to the range [0, 2], then masked outside the unit pupil to emphasize the valid interferometric region. This consistent visual treatment enables clear comparison of aberration effects across the animated sequences.

3 Results

The simulation generated interference patterns for seven aberration cases under flat and wedged plate configurations, as well as a dynamic GIF for defocus evolution. Key findings include:

• **Ideal Plane**: Fig. 1 illustrates the comparison between a perfect plane wavefront and a wavefront with a linear phase introduced by a wedged plate tilted at $10^{-3}x$ (m). The left panel shows a uniform circular intensity distribution, characteristic of a constant phase light wave superposition, while the right panel exhibits parallel interference fringes resulting from the tilt. Intensity is depicted in arbitrary units on a 0–2 scale.

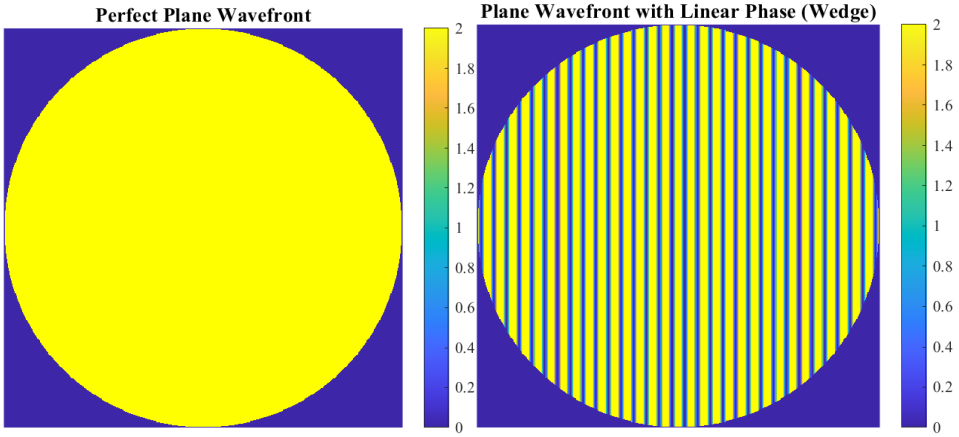

Figure(1). Perfect Plane Wavefront and Wavefront With Wedge

• **Defocus**: Fig. 2 compares a perfect plane wavefront with defocus and a wavefront with defocus combined with a slight wedge angle. The left panel displays concentric, curved fringes typical of defocus, while the right panel shows additional interference fringes induced by the wedge tilt. Intensity is represented in arbitrary units on a 0–2 scale, with axes labeled in millimeters.

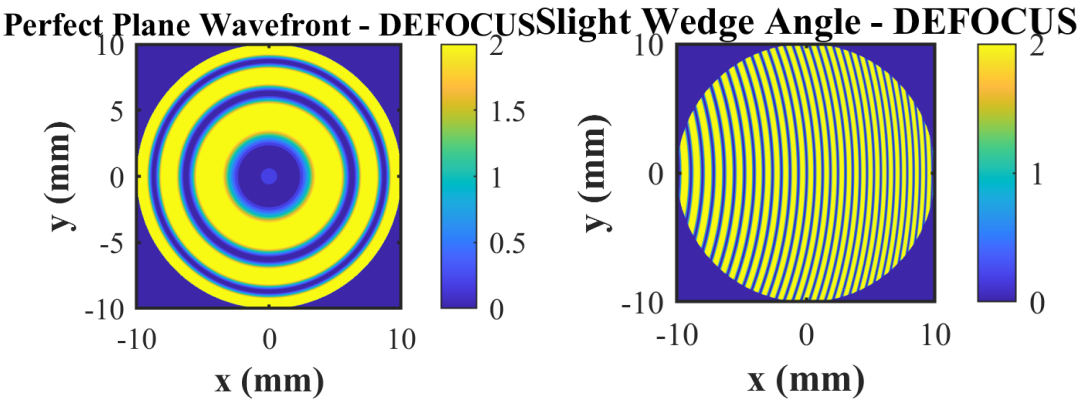

Figure(2). Plane Wavefront and Wedge Angle in Defocus Situations

• **Horizontal and Vertical Coma**: Fig. 3 compares the interference patterns of horizontal (HCOMA) and vertical (VCOMA) coma under perfect plane wavefront and slight wedge angle conditions. The upper figures display the characteristic coma fringes, with HCOMA showing vertical patterns and VCOMA exhibiting parallel patterns. The lower figures illustrate the modified patterns when a slight wedge angle is introduced, results become more complex. Intensity is represented in arbitrary units on a 0–2 scale, with axes labeled in millimeters.

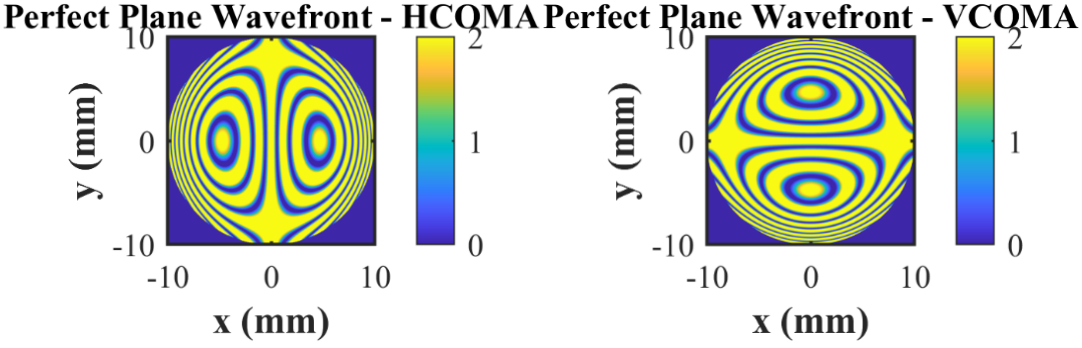

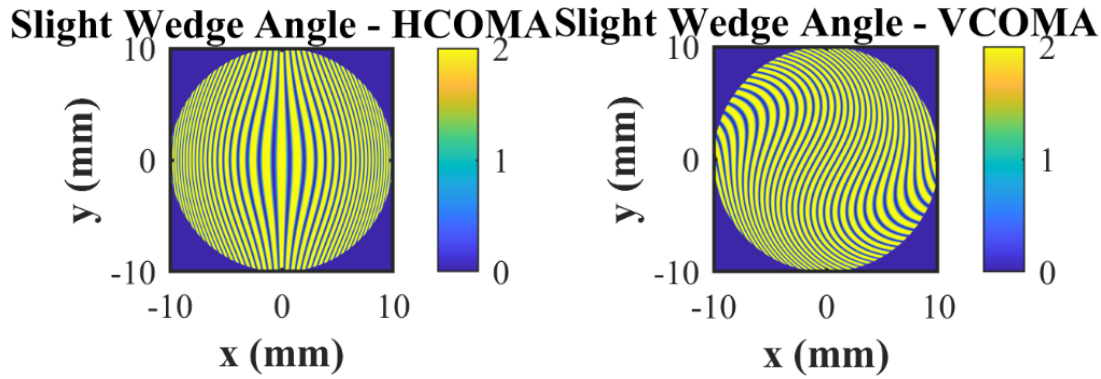

Figure(3). Parallel Coma and Vertical Coma in Parallel and Wedge Angle Situations

• **Spherical Aberration**:

Fig. 4 presents the interference patterns for spherical aberration under perfect plane wavefront and slight wedge angle conditions. The left panel exhibits circular radial interference fringes typical of spherical aberration in a plane wave, while the right panel shows more complex fringes symmetric along the x-axis, resulting from the introduction of a wedge angle. Intensity is depicted in arbitrary units on a 0–2 scale, with axes labeled in millimeters, illustrating the effect of the wedge on the spherical aberration pattern.

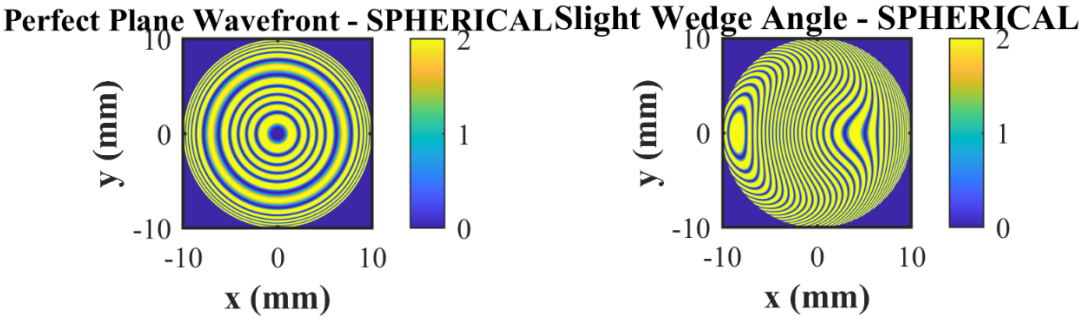

Figure(4). Plane Wavefront and Wedge Angle in Spherical Situations

• **Astigmatism 0°and 45°**: Fig. 5 displays the interference pattern for astigmatism, featuring elliptical fringes aligned with a slight wedge angle. The upper figures show a perfect plane wavefront with astigmatic contours, while the lower figures illustrate the superimposition of linear fringes due to the wedge plate, enhancing the complexity of the pattern. Intensity is represented in arbitrary units on a 0–2 scale, with axes labeled

in millimeters.

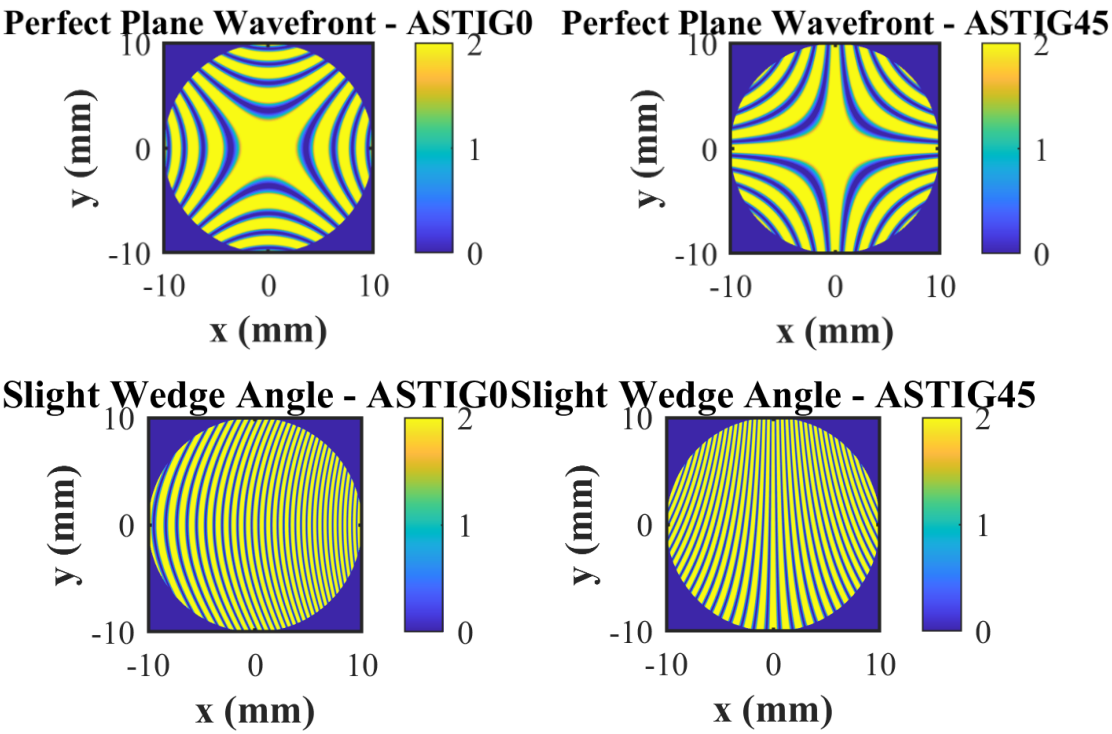

Figure(5). Plane Wavefront and Wedge Angle in astigmatism Situations

• **Dynamic Defocus**: The GIF showed a smooth transition from negative defocus (concave fringes) to positive defocus (convex fringes), with fringe curvature increasing with amplitude, detailing frames have been shown in Part2.4.

All patterns were confined to the 20 mm circular aperture, with intensities range $[0,2]$. The wedged plate consistently introduced additional changes compared to the flat plate.

4 Discussion

The simulation successfully reproduced the expected interference patterns for Zernike aberrations, validating its ability to model wavefront distortions in a lateral shearing interferometer. The ideal plane case confirmed the baseline behavior, with uniform fringes for the flat plate and linear fringes for the wedged plate, consistent with theoretical expectations [2]. Aberration specific patterns (e.g. concentric fringes for

defocus, comet-like fringes for coma) matched the characteristic shapes of Zernike polynomials, confirming the accuracy of the OPD calculations.

The wedged plates linear tilt introduced additional phase gradients, resulting in more complex patterns that highlight the interferometers sensitivity to both aberration and tilt. The dynamic defocus simulation demonstrated the continuous evolution of fringe patterns, providing a visual tool for understanding aberration effects over a range of amplitudes.

These results validate the simulations utility in addressing the problem of wavefront characterization. The distinct fringe patterns for each aberration enable identification and quantification of wavefront distortions, supporting applications in optical testing and adaptive optics. The dynamic GIF further illustrates the ability of interferometer to track changing aberrations, relevant for real-time correction systems.

Future work could extend the simulation to include multiple shear directions, variable wavelengths, or higher-order Zernike terms. Additionally, incorporating noise models or experimental data could enhance realism, bridging the gap between simulation and practical implementation.

References

[1] Malacara, D. (2007). Optical Shop Testing, 3rd ed. Wiley.
[2] Murty, M. V. R. K. (1964). The use of a single plane parallel plate as a lateral shearing interferometer. Applied Optics, 3(4), 531–534.
[3] Zernike, F. (1934). Diffraction theory of the knife-edge test and its improved form, the phase-contrast method. Monthly Notices of the Royal Astronomical Society, 94, 377–384.